Arabian Journal of Chemistry (2023) **16**, 104837

King Saud University

Arabian Journal of Chemistry

www.ksu.edu.sa
www.sciencedirect.com

ORIGINAL ARTICLE

Controlled removal of fluoride by ZIF-8, ZIF-67, and Ni-MOF of different morphologies

Amir Afarinandeh [a], Kambiz Heidari [a], Mariusz Barczak [b], Magda H. Abdellattif [c], Zahra Izadi Yazdanaabadi [d], Ali Akbar Mohammadi [e], Gholam Ali Haghighat [f,*], Mahmoud Shams [g,h,*]

[a] *Department of Chemical Engineering, Payame Noor University, Tehran, Iran*
[b] *Institute of Chemical Sciences, Faculty of Chemistry Maria Curie-Skłodowska University in Lublin, 20-031 Lublin, Poland*
[c] *Department of Chemistry, College of Science, Taif University, Turaba Branch P.O. Box 11099, Taif 21944, Saudi Arabia*
[d] *Student Research Center, Jiroft University of Medical Sciences, Jiroft, Iran*
[e] *Department of Environmental Health Engineering, Neyshabur University of Medical Sciences, Neyshabur, Iran*
[f] *Department of Environmental Health Engineering, School of Health, Jiroft University of Medical Sciences, Jiroft, Iran*
[g] *Social Determinants of Health Research Center, Mashhad University of Medical Sciences, Mashhad, Iran*
[h] *Department of Environmental Health Engineering, School of Health, Mashhad University of Medical Sciences, Mashhad, Iran*

Received 23 December 2022; accepted 19 March 2023
Available online 23 March 2023

KEYWORDS

MOFs;
ZIFs;
Ni-MOF;
Fluoride;
BBD Modeling

Abstract As an emerging class of nanoporous materials, Metal Organic Framework (MOFs) are distinguished for environmental remediation. ZIFs and Ni-MOF chosen as fluoride (F^-) scavengers due to their robust structures and straightforward synthesis routes. F^- adsorption was studied as a function of the ZIFs geometry and structural properties. The efficacy of MOFs for F^- abatement was in the order of ZIF-67-NO3 (70.1%) > ZIF-8-Cube (64.7%) > ZIF-67-OAc (62.4%) > ZI F-8-Cuboid (59.2) > Ni-MOF (58.5%) > ZIF-8-Octahedron (57.1%) > ZIF-8-Leaf (55.3%) > ZIF-67-SO4 (55.1%) > and ZIF-67-Cl (52.3%). The key operating variables i.e. pH, mixing time, F^- concentration, and ZIF-67-NO3 dose were modeled using the Box-Behnken design (BBD). The model revealed the process mainly influenced by solution pH. The model optimized the operating condition and obtained a maximum 85.9% F^- removal by mixing time = 41.1 min, ZIF-67-NO3 dose = 0.9 g/L, solution pH = 4.86, and F^- = 6.5 mg/L. Non-linear form of isotherm and kinetic models disclosed the multilayers F^- adsorption onto ZIF-67-NO3 with an qmax = 25.9 mg/g, and chemisorption as the rate-controlling step. F^- sorption decreased slightly by temperature in the

* Corresponding authors.
E-mail addresses: gha.haghighat@jmu.ac.ir (G.A. Haghighat), shamsmh@mums.ac.ir (M. Shams).
Peer review under responsibility of King Saud University.

Production and hosting by Elsevier

https://doi.org/10.1016/j.arabjc.2023.104837

range of 303 to 323 K. The structure of ZIF-67-NO3 remained stable under three consecutive use-reuse cycles with an about 10% loss in removal efficiency.

1. Introduction

Contamination of waterbodies with fluoride (F^-) has been recognized as a major concern that impacted the quality of life of millions of people across the universe. World Health Organization and the U.S. Environmental Protection Agency set a guideline and maximum acceptable concentration (MCL) of 1.5 mg/L, and 4 mg/L, respectively to prevent noncarcinogenic health effects of F^- (Council 2007, Edition 2011). Studies revealed a substantial statistical correlation between a variety of health issues such as lower children's IQ (Till et al. 2020), fluorosis, and damage to the liver and kidney with an excessive F^- intake (Yang &Liang 2011). As drinking water is the major route for F^- intake, the presence of this contaminant in potable water was being a challenge for many water suppliers. Accordingly, the removal of excessive F^- from drinking water is the key point to preventing F^- related diseases.

Until now, many treatment techniques including coagulation, precipitation, ion exchange, electrocoagulation, membrane separation, and dialysis have been used against F^- contamination (Karunanithi et al. 2019, Mohapatra et al. 2009). Among different techniques, adsorption is a versatile technique for the removal of a variety of contaminants (Acharya et al. 2018, Nazir et al. 2022b, Rasoulzadeh et al. 2021a, Rasoulzadeh et al. 2021b). The reusability of materials, efficient utilization of space, compatibility of the treatment system for low contaminant levels, availability of different adsorbents, and the dynamic nature of adsorption science, make this process an interesting and viable option (Li et al. 2018, Soltani et al. 2019). Studies are extensively conducted to improve adsorbent characteristics i.e. adsorption capacity, surface area, selectivity, and reusability.

The development of metal–organic frameworks (MOFs) in recent decades opened a new avenue in the world of material science. MOFs are composed of metallic parts connected by organic linkers to build uniform geometrical structures (Anik et al. 2019, Esrafili et al. 2022, Safaei et al. 2019). The structure of MOFs and their functionalities could be engineered to acquire exceptional properties. These advantages put MOFs at the focal point of a variety of research fields such as separation, gas purification, catalysis (Konnerth et al. 2020, Kumar et al. 2022), water splitting (Shah et al. 2022), sensing, drug delivery, and energy generation and storage (Chueh et al. 2019, Van Nguyen et al. 2022). Of interesting and modern applications of MOFs are the use of MOFs for the degrading and recycling PET wastes (Yang et al. 2021), and blue energy production by modern osmotic membrane(Liu et al. 2021). Various MOFs were also successfully synthesized and applied for the adsorption of contaminants such as dyes (Haghighat et al. 2020, Oveisi et al. 2018), heavy metals (Feng et al. 2018), pesticides, and antibiotics (Khan et al. 2021, Nazir et al. 2021) (Dehghan et al. 2019).

Nickel, zinc, and cobalt-based frameworks are among the water-stable MOFs that attract attention for a variety of applications (Nazir et al. 2022c). ZIFs and Ni-MOFs were successfully incorporated into the membrane structures to improve characteristics such as selectivity and durability (Song et al. 2019). As adsorbents, these MOFs are applied for the removal of contaminants i.e. antibiotics and pharmaceutical intermediates (Abdelhameed &Emam 2019, Liang et al. 2018), heavy metals (Bo et al. 2018), radionucleotide (Li et al. 2020), environmental toxicants (Andrew Lin &Lee 2016), and dyes such as crystal violet, methyl orange (Nazir et al. 2020), malachite green (Lin &Chang 2015) and Congo red (Yang &Bai 2019).

Up to now and to the best of our knowledge, limited studies have been conducted on herein-studied MOFs for their F^- adsorption. In a study on ZIF-8 nanoparticles (Pillai et al. 2019) by Pillai et al, rapid uptake of F^-within 15 min was obtained and researchers reported a promising capacity of 90 mg/g. However, the synthesis route for ZIF-8 preparation was different from those we proposed in this study. Kamarehie et al. (Kamarehie et al. 2018) and Khoshnamvand et al (Khoshnamvand et al. 2019) also studied ZIF-8 as F^- scavengers and found the highest capacity of 25 mg/g, and 33 mg/g, respectively.

Herein, we cover scientific gaps exist based on the literature review on fluoride removal onto MOFs. Up to now and to the best of our knowledge, there is no published literature on the study of F^- adsorption by Ni-MOFs and ZIF-67. Moreover, the F^- adsorptive properties as a function of the geometrical structures of ZIF-67 and ZIF-8 were not yet studied. Herein, we followed a simple and high throughput synthesis protocol to prepare ZIFs at room temperature. Ni-MOF was prepared via a solvothermal route. The prepared materials were investigated for their adsorptive properties for F^-. A systematic approach, response surface methodology (RSM), was opted to study the effect of major operating variables i.e. pH, contact time, F^- concentration, and MOF dose on the process. RSM is an advanced statistical strategy to design the study framework that is superior to the traditional one-factor-at-a-time (OFAT) approach in many ways. For adsorption systems, RSM provides a useful tool to determine the interactions between variables and their non-linear effects on adsorption efficiency. Moreover, the prediction of removal efficiency under determined environmental conditions becomes feasible by the model developed by regression analysis (Asgari et al. 2022, Mohammadi et al. 2017a, Nezhad et al. 2020). In addition, the polynomial model could optimize the process for the highest removal. The kinetic and the equilibrium of F^- adsorption by non-linear models, effect of temperature, and reusability of adsorbent also studied and presented in this work.

2. Experimental

2.1. Chemicals and reagents

The chemicals and precursors used for MOFs synthesis and experimental tests were AR grade. Deionized water (DI, EC < 0.5) and DMF (99.8%) were used as solvents for the synthesis. Terephthalic acid (TPA, 98%) and 2-Methylimidazole (HMIM, 99%) were used as organic linkers. $Zn(OAc)_2$ (98%) and $Zn(NO_3)_2{\cdot}6H_2O$ (>99%) are also used as metal sources for MOFs preparation.

2.2. Synthesis of MOFs

The details of MOF synthesis as described in the literature are presented in the following.

Ni-MOF: 2 mmol of each Ni-MOF precursors, $Ni(NO3)_2$, and TPA, added to a mixture of 35 mL DMF, 2.5 mL ethanol and 2.5 mL DI. The mixture mixed well for 30 min to yield a clear solution and then transferred to a Teflon-lined autoclave at 125 °C for 720 min (Yang &Bai 2019).

Cubic ZIF-8: 0.594 g $Zn(NO_3)_2{\cdot}6H_2O$ and 0.328 g HMIM added to 3 mL of DI and 3.76 g of NH_3 solution, separately. The colorless zinc nitrate solution then added to HMIM solution and the mixture agitated for 10 min (Liu et al. 2015b).

Dodecahedral ZIF-8: 0.863 g $Zn(OAc)_2$ and 11.35 g HMIM dissolved in 8 mL and 80 mL DI, respectively. The metal

solution then added gently to ligand solution and stirring continued for further 4 h for crystallization.

Leaf ZIF-8: 0.59 g of $Zn(NO_3)_2{\cdot}6H_2O$ and 1.3 g of HMIM were added to 40 mL deionized water, separately. After clear solutions formed, they mixed and the solution stirred for 4 h.

Cuboid ZIF-8: 1.3 g of HMIM dissolved in 40 mL distilled water containing 200 mg of Polyvinylpyrrolidone (PVP). Second solution was prepared by dissolving 0.595 g of $Zn(NO_3)_2{\cdot}6H_2O$ in distilled water. The two solutions were mixed and the crystallization completed within 30 min.

ZIF-67: Synthesis of ZIFs with different metal sources led to the formation of crystals with different morphology and structural properties. 1.642 g of HMIM and 1 mmol of cobalt salts ($CoSO_4$, $Co(OAC)_2$, $CoCl_2$, and $Co(NO_3)_2$) dissolved separately in 10 mL of DI. The clear solutions were mixed and stirred for 30 min (Guo et al. 2015). The solutions turn to violet instantly after the metal and linker solutions mixed together.

After the completion of the synthesis, MOF crystals were separated from the suspensions by centrifugation, washed thoroughly with distilled water (ZIFs), and dried overnight at 70 °C before use.

2.3. Adsorbent characterization

The structural properties and the soundness of synthesis routes were confirmed by scanning electron microscope (SEM) by MIRA3 TESCAN, Czech Republic, and Fourier-transform infrared spectroscopy (FTIR) using a Thermo Nicolet, Avatar 370 spectrophotometer. The BET surface areas of MOFs were also presented and discussed as a functional variable that affects F^{-1} removal.

2.4. Adsorption experiments

Batch mode experiments were opted to compare MOF's adsorptive properties and to determine how operating variables govern the F^- uptake. Flasks containing 50 mL solutions with an adjusted F^- concentration, solution pH, and MOF mass (based on BBD design in Table 3) were used for the experimentations. The mixtures were stirred at 250 rpm for the specified time and finally, the suspensions were centrifuged at 5000 rpm for 10 min. The residual F^{-1} concentration in the supernatant was determined by the standard SPADNS approach using a UNICO UV-2100 spectrophotometer at 570 nm. The process responses i.e. F^- removal percentage (μ), and adsorption capacity were calculated by the equations described in the supplementary.

2.5. Screening MOFs for F^- adsorption

The synthesized MOFs were evaluated to realize the comparative adsorption affinity of F^- and to screen the material with the highest removal potential. A specified mass of MOFs was added to the solutions containing 10 mg/L F^{-1} and the solutions were well mixed for 30 min. The adsorptive potential of MOFs was analyzed by calculating adsorption capacity and removal efficiency. The MOF with superior adsorptive properties then undergoes a series of additional standard-designed experiments for process modeling and optimization.

2.6. F^- adsorption modeling, optimization, and validation

Box-Behnken design (BBD) was adopted to systematically design the experiments. The BBD is a response surface method (RSM) that studies the variables at 3-levels. Compared to other RSM methods, BBD design has obvious advantages such as ease of factors adjustment (pH, adsorbent dose, and sorbate concentration), and a lower number of required tests. The variables and their herein studied levels are presented in Table 1.

Considering the variables in Table 1, a design matrix was developed by Design Expert software (version 12) composed of a total of 29 runs, of which 5 runs were set at center points. The standard replications at center points are crucial to estimate the experimental error and model validation. After performing the experiments in the designed order, analysis of variance (ANOVA) was used to find the best-fit model among linear, 2Fl, quadratic, and cubic models.

The best model select based on the statistical parameters to give a suitable prediction for F^{-1} removal under specified operational conditions. The model then optimized to determine the condition for the highest F^{-1} adsorption. Finally, the optimal condition validated by performing the experiments under simulated conditions.

2.7. Kinetic and isotherm studies

To elucidate the mechanism govern the adsorption and to assessing the dynamic characteristics of the sorption system, the kinetic and isotherm studies are essential. Kinetic data was collected by analyzing F^{-1} removal over time while all variables (except time) were adjusted at their optimum level. The data then analyzed with a non-linear form of four known kinetic models, the pseudo-first-order (PFO), the pseudo-second-order (PSO), intraparticle diffusion, and the Elovich models.

The adsorption capacity at the equilibrium for different sorbate concentrations were used to isotherm modeling. For equilibrium study, pH and MOF mass were adjusted at the optimum levels and the solution were mixed for 8 h. Seven common isotherm models e.g. Langmuir, Temkin, Sips, Freundlich, Toth, Redlich-Peterson, and Khan were applied to simulate the experimental data. The nonlinear models and statistical parameters i.e. R^2_{Adj}, R^2, and sum of squares error (SSE) described in the supplementary were checked to find out the best fit models.

Table 1 Range and levels of independent variables in the study of F^- removal by MOFs.

Factor	Code value	level		
		−1	0	+ 1
Mixing time (min)	A	15	37.5	60
Adsorbent (g/L)	B	0.4	0.7	1
pH	C	4	7	10
F^{-1} (mg/L)	D	4	7	10

2.8. Effect of temperature

Solution temperature could affect the process efficiency and is crucial to study for operating the water/wastewater treatment units. The experiments accomplished under optimal condition where the solution temperature varied in the range of 303 to 323 K. The data then analyzed to identify whether the nature of the adsorption is endothermic or exothermic.

3. Results and discussion

3.1. Adsorbent characterization

The synthesized materials are among the known and stable forms of MOFs with exceptional geometrical morphology. Fig. S1 shows the SEM images of as-synthesized MOFs. The figure clearly shows the precise truncated rhombic dodecahedral structures for ZIF-67-OAc and ZIF-67-SO4 crystals. ZIF-67-NO3 and ZIF-67-Cl crystals have rhombic dodecahedrons structures with a narrow size distribution, however, the latter has rough surface particles. As implied from the names and shown in the figure, ZIF-8-Cuboid, ZIF-8-Octahedron, ZIF-8-Cuboid, and ZIF-8-Leaf have regular geometrical structures, which are consistent with those reported earlier. Moreover, the XRD pattern of as-synthesized MOFs depicted in Fig. 1. All characteristic peaks for ZIFs and Ni-MOF match well with those reported in the literature (Guo et al. 2015, Huang et al. 2017, Yang &Bai 2019).

The composition of as-synthesized MOFs was investigated by FTIR and the obtained results are presented in Fig. 2 (a-i). All the obtained MOFs have similar spectra due to the same assembling forces between 2-methylimidazole (HMIM) organic linker and zinc atoms in the obtained ZIF MOFs. Most of the observed peaks can be assigned to the stretching and bending vibrations of 2-methylimidazole including vibrations bands at 1578 cm^{-1} (C = N stretching), 1412 cm^{-1} (CH_3 bending), 1306 cm^{-1}, 1146 cm^{-1}, and 994 cm^{-1} (in-plane bending modes of the HMIM ring), 748 cm^{-1} and 690 cm^{-1} (out-of-plane aromatic C–H bending) (Liu et al. 2015b, Pillai et al. 2019).

Bands located at $\sim$ 2900–3100 cm^{-1} can be attributed to the C–H stretching modes of the aliphatic methyl group and imidazole ring present in the HMIM linker, respectively

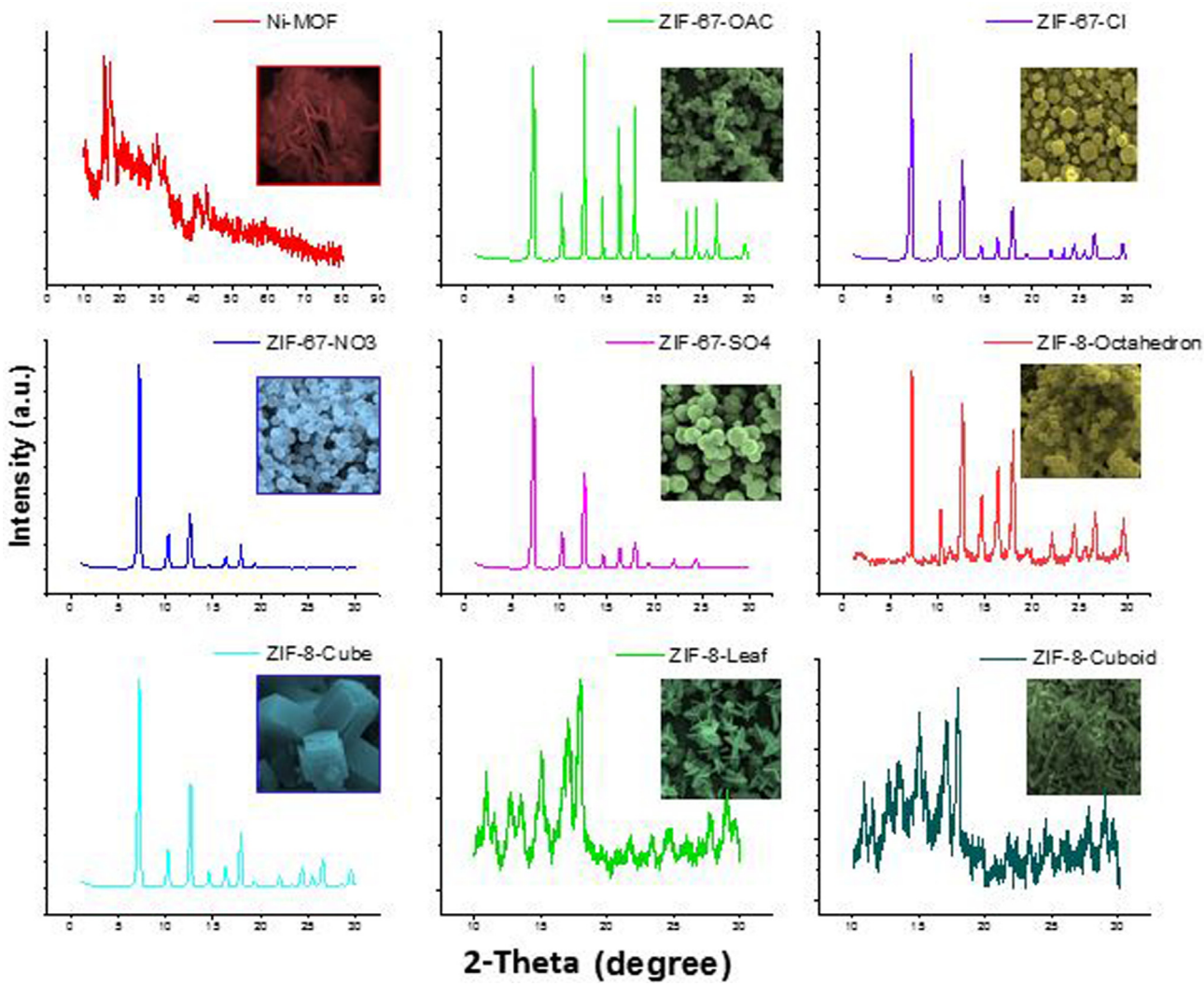

Fig. 1 The XRD pattern of as-synthesized MOFs.

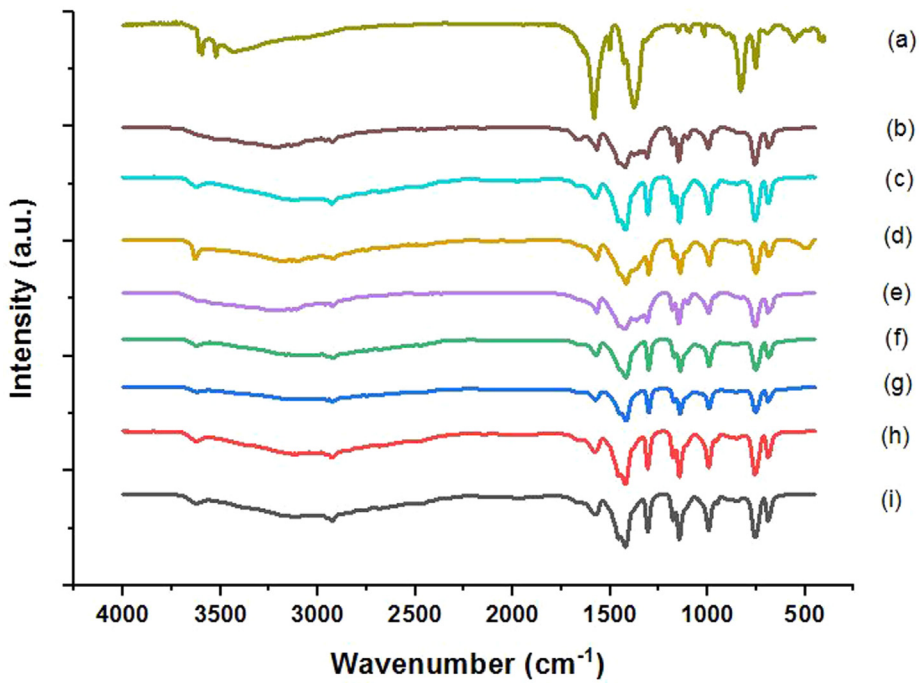

Fig. 2 The FTIR spectra of Ni-MOF (a), ZIF-8-Cuboid (b), ZIF-8-Octahedron (c), ZIF-67-NO3 (d), ZIF-8-Cube (e), ZIF-67-SO4 (f), ZIF-67-OAC (g), ZIF-8-Leaf (h), ZIF-67-Cl (i).

(Khan et al. 2018). Additional discussion on FTIR of ZIF-67-NO3 before and after F^- adsorption is available in the supplementary.

3.2. Effect of MOF type

MOFs are promising materials due to the potential for adopting different routes and precursors for synthesis which consequently yield MOFs with different morphologies and adsorptive characteristics. ZIF-67 and ZIF-8 are good examples on the role of the mole ratio of the linker to metal ions, and metal source in the morphology, structural properties, and adsorptive characteristics of MOFs. Table 2 lists the physical properties of as-synthesized MOFs. The table also shows the adsorption efficiencies of MOFs for F^-. As seen, ZIF-67-NO_3 shows superior efficiency compared to other studied MOFs and chosen for further studies i.e. BBD modeling, optimization, kinetic, isotherm, and reusability tests. The affinity of F^- to adsorb onto MOFs was decreased in the order of ZIF-67-NO3 > ZIF-8-Cube > ZIF-67-OAc > ZIF-8-Cuboid > Ni-MOF > ZIF-8-Octahedron > ZIF-8-leaf > ZIF-67-SO4 > and ZIF-67-Cl. ZIF-67-NO3 has a lower SSA and pore volume compared to many studied MOFs hence the F^- adsorption was not significantly affected by the morphology and SSA. Liu et al also synthesized ZIFs with three morphologies (cubic, leaf-shaped and dodecahedra) for arsenic removal. The authors concluded that neither SSA nor morphology was determining factor for ZIFs adsorptive properties based on the kinetics and isotherm models (Liu et al. 2015a).

3.3. BBD modeling of F^- adsorption

To model the effect of four variables i.e. contact time (A), ZIF-67-NO3 (B), solution pH (C), and F^- concentration (D) on F^- removal efficiency, an experimental matrix developed consisting of 29 runs. The experimental runs and the corresponding F^- adsorption percentages are presented in Table 3.

The ANOVA of F^- experimental removal in Table 3 as a function of coded variables yielded a polynomial quadratic model as follows:

Table 2 The structural properties of MOFs (Guo et al. 2015, Huang et al. 2017, Yang &Bai 2019) and their F^- removal efficiencies.

MOFs	ligand	Metal source	Crystal shape	BET SSA (m^2/g)	Pore volume (cm^3/g)	F^- removal
ZIF-67	HMIM	$Co(NO_3)_2$	Rhombic dodecahedron	734	0.34	70.1 ± 2.5
	HMIM	$Co(OAC)_2$	Truncated rhombic dodecahedral	1323	0.57	62.4 ± 1.8
	HMIM	$CoSO_4$	Truncated rhombic dodecahedral	1375	0.62	55.1 ± 1.9
	HMIM	$CoCl_2$	Rhombic dodecahedron	1278	0.52	52.3 ± 2.2
ZIF-8	HMIM	$Zn(NO_3)_2$	Octahedron	1151	0.58	57.1 ± 3.4
	HMIM	$Zn(OAc)_2$	Leaf shape	12.7	0.04	55.3 ± 1.2
	HMIM	$Zn(NO_3)_2$	Cuboid	890	0.48	59.2 ± 1.6
	HMIM	$Zn(NO_3)_2$	Cube	978	0.51	64.7 ± 1.5
Ni-MOF	TPA	$Ni(NO3)_2$	Flower like	63	0.31	58.5 ± 2

Table 3 BBD design matrix and corresponding F^- removal by ZIF-67-NO3.

Run No	Coded variable				% Removal	Run No	Coded variable				% Removal
	A	B	C	D			A	B	C	D	
1	37.5	0.7	7	7	78.1	16	37.5	1	7	4	80.5
2	37.5	0.7	10	4	54.6	17	15	0.4	7	7	53.7
3	60	1	7	7	75.1	18	37.5	0.7	7	7	81.2
4	37.5	0.7	4	10	81.3	19	37.5	0.4	10	7	46.1
5	15	0.7	4	7	72.2	20	37.5	0.7	7	7	77.4
6	37.5	0.7	7	7	79.8	21	37.5	0.7	7	7	76
7	60	0.7	4	7	79.3	22	15	1	7	7	66.5
8	37.5	0.4	7	4	69.6	23	37.5	0.7	10	10	41.4
9	60	0.7	7	4	79.8	24	15	0.7	7	4	63.1
10	37.5	1	7	10	65.6	25	37.5	1	4	7	88.4
11	15	0.7	7	10	58.8	26	15	0.7	10	7	35.1
12	37.5	0.4	4	7	73.2	27	60	0.7	7	10	70.3
13	37.5	1	10	7	54.7	28	37.5	0.7	4	4	75.2
14	60	0.4	7	7	78.8	29	37.5	0.4	7	10	61.9
15	60	0.7	10	7	62.5						

$$F^- removal = 78.50 + 8.03A + 3.96B - 14.60C - 3.63D - 4.12AB + 5.08AC - 1.80BD - 4.82CD - 6.00A^2 - 3.64B^2 - 9.90C^2 - 5.14D^2 \quad (1)$$

The model based on the coded values could be used to compare the significance of different variables on response. According to Eq. (1), solution pH (C) has the highest coefficient and thus the most influential variable on F^- adsorption efficiency. In a study on MIL-101(Al) that designed by response surface methodology, Yang et al reported the pH as the largest influencing factor on F^- removal (Yang et al. 2022). The negative sign of model term in the equation indicated that the adsorption decreased by increasing the factor level. Hence, the F^- removal decreased significantly by pH and F^- concentration and increased by time and ZIF-67-NO3 mass added to the solutions.

The major statistical parameters that mirror the adequacy of the model for predicting the F^- removal as operating variables change are presented in Table S1. For a good model, the R^2 (coefficient of determination) would be beyond 0.8, and the difference between $R2_{adj}$ and predicted R^2 values should be < 0.2 (Saghi et al. 2020). The adequacy of the model to predict the removal efficiency is also obvious in Fig. 3 where the experimental removal are distributed uniformly close to the regression line.

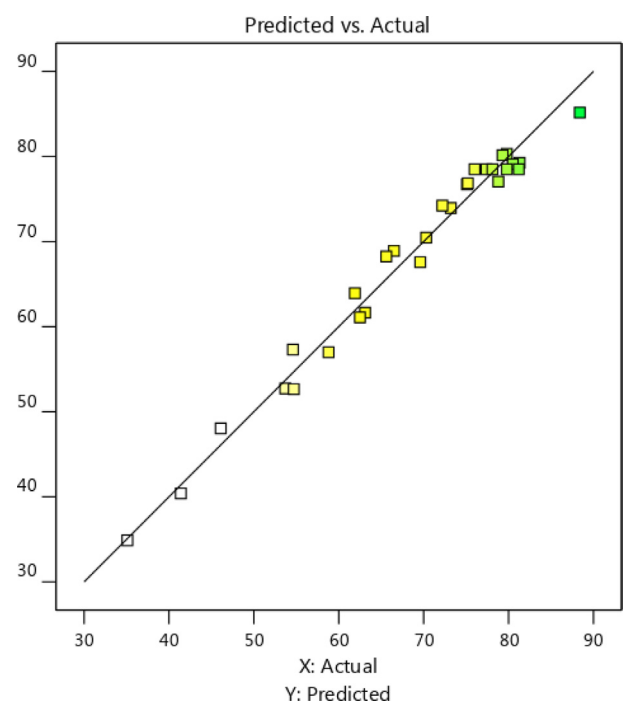

Fig. 3 The distribution of experimental F^- removal versus those predicted by the model.

3.4. Effects of model terms and their interactions

3.4.1. Effect of adsorbent dose

The mass of adsorbent used for the removal of a tatgeted contaminant is crucial for the successful design of the cost-effectiveness of the whole process. Herein, F^- removal was monitored as a response to varying ZIF-67-NO3 doses applied in the range of 0.4 g/L to 1.0 g/L. Fig. 4 (a, c) shows the F^- removal slightly increased when a higher mass was applied to the solutions. Similar observations were reported in the adsorption of erythromycin (Gholamiyan et al. 2020), Pb(II) (Rasoulzadeh et al. 2020), basic Fuchsin dye (Ba Mohammed et al. 2020), and phosphate (Mazloomi et al. 2019). It is well understood that the available sorption sites in the solution increased by adsorbent dose and hence more vacant sorption sites exist for contaminants removal (Ba Mohammed et al. 2020). Due to the economic considerations in real treatment systems, however, exploring the optimal adsorbent dose is critical.

3.4.2. Effect of pH

pH is a critical factor in sorption systems as it determines the charge of contaminants, competing ions, and adsorbent surface in the solution. In this study, the effect of pH in the range of 4–10 was studied by adjusting the pH of the F^- solutions using 0.1 and 0.01 N HCl or KOH. As shown in Fig. 4 (b),

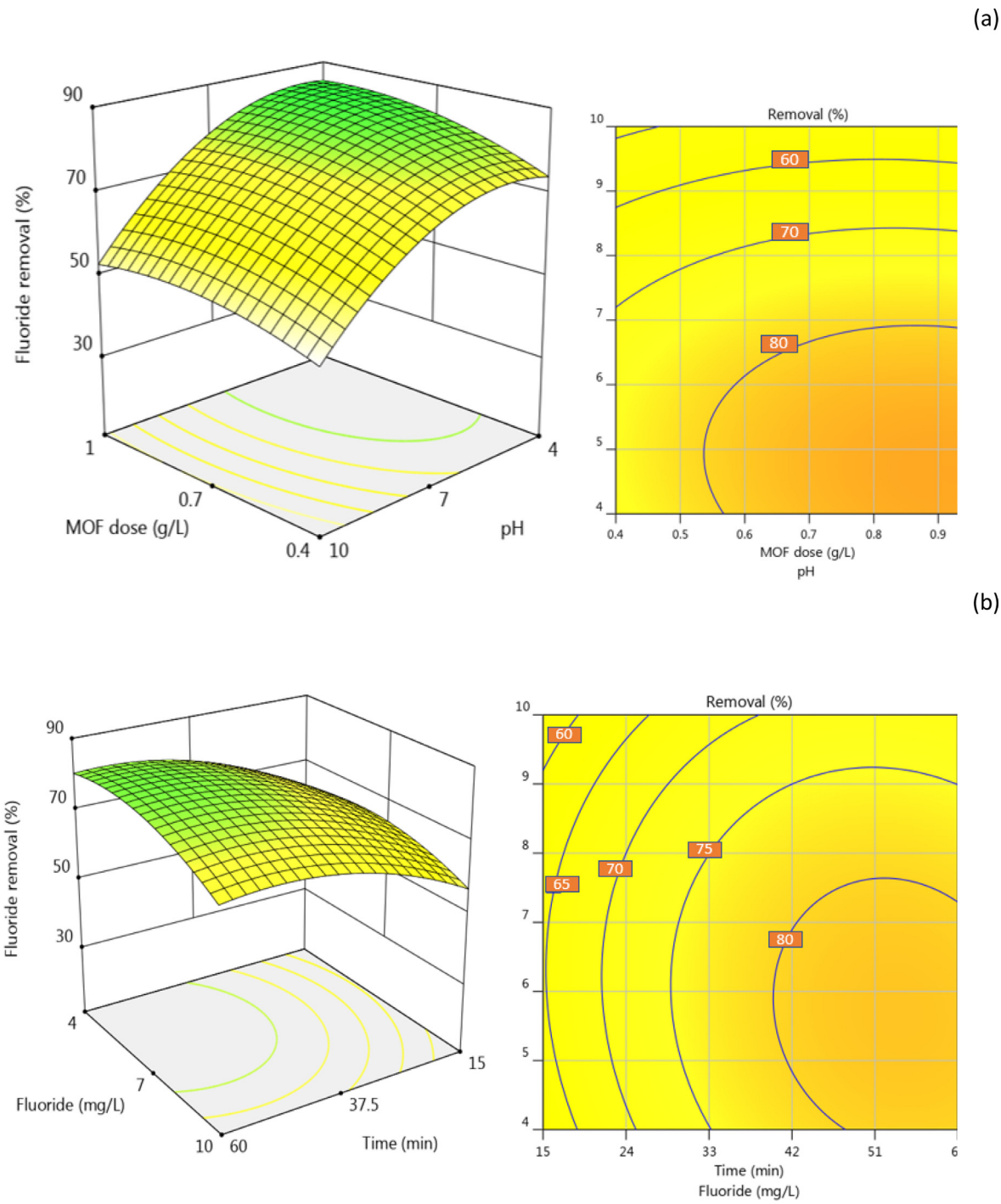

Fig. 4 F^- removal behavior by operating variables. The effect of MOF dose and solution pH (a), mixing time and F^- concentration and (b), and MOF dose and mixing time (c).

the solution pH shows a significant influence on F^- adsorption, and the removal increased from about 42 to 74% by increasing pH from 4 to 10. These findings could be explained by the competence between the negatively charged ions of F^- and hydroxyl ions at elevated pH. The increasing F^- removal at low pH, on the other hand, was a consequence of the domination of attraction force between F^- and the positively charged surface of ZIF-67-NO3. The isoelectric pH of ZIF-67-NO3 is about 8.7 that means the surface of MOF gets more positive charges by decreasing the solution pH from 8.7. Our findings are in agreement with other studies on phosphate adsorption onto ZIF-8 (Mazloomi et al. 2019) and F^- removal by MOF-801 (Zhu et al. 2018) where the authors attributed the low removal efficiencies to the presence of hydroxyl ions at alkaline solutions.

3.4.3. Contact time

Contact time is a key factor in the design and operation of treatment units. It is also an essential parameter that governs

(c)

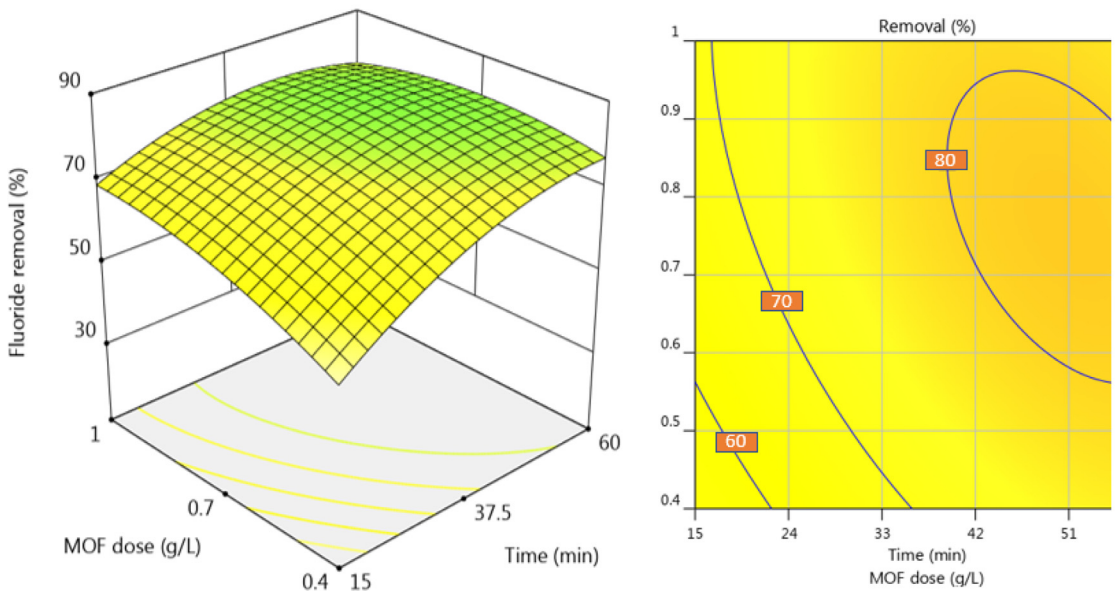

Fig. 4 (*continued*)

the economy of treatment systems by determining the volume of the treatment unit and energy demand. Fig. 4 (b, c) shows the F^- removal by ZIF-67-NO3 over time. As seen, a significant F^- removal of about 55 % observed in the first 15 min of mixing time and increase up to 70–80 % in the first 60 min. Rapid adsorption at the beginning of adsorption process has been previously reported for cationic dye due to the high driving force and access of adsorbate to available sorption sites (Ahamad et al. 2019). Some authors attributed this behavior to the presence of the higher numer of available sorption sites at the initial stage of the process which are gradually being occupied by contaminant ions (Liu et al. 2015b, Mazloomi et al. 2019).

3.4.4. Effect of initial F^- concentration

F^- concentrations up to 10 mg/L were commonly reported in the groundwaters around the globe (Moghaddam et al. 2018, Mohammadi et al. 2017b). Thus, in this study, F^- removal by ZIF-67-NO3 was studied on solutions contained F^- in the range of 4 mg/L to 10 mg/L. Fig. 4 (b) shows the removal efficiency as a function of F^- concentration. As seen, F^- removal decreased under higher F^- concentrations that can attributed to the competence between the F^- ions to adsorb on the surface and also repellent force between F^{-1} ions at high concentrations. Similar findings reported by Massoudinejad et al on F^{-1} removal using UIO functionalized with amine in the range of 10 mg/L to 25 mg/L. They explained the high removal to the presence of adequate adsorption sites for low F^{-1} concentrations (Massoudinejad et al. 2016).

3.5. Model optimization and validity tests

One major goal in modeling various sorption processes is to figure out the optimal condition in which the highest removal could be achieved. Solving Eq. 4 to calculate the independent variable levels for highest F^- removal showed a maximum 85.9% F^- removal by adjusting the mixing time to 41.1 min, ZIF-67-NO3 dose to 0.9 g/L, solution pH to 4.86, and F^- concentration to 6.5 mg/L. To experimentally examine this theoretical condition, the optimum condition was simulated and F^- removal was studied in triplicate. The average F^- removal was 86.5% ± 2.7 which is consistent with the value predicted by the model.

3.6. Isotherm and kinetic studies

Equilibrium data obtained by conducting the experiments under the optimal condition in section 3.5., were fitted by the most recognized non-linear isotherm models listed in Table S2. The results of isotherm modeling presented in Table S3, and Fig. 5. As seen, the table shows a higher R^2, R^2_{Adj} and smaller RSS for the Freundlich model compared to other models. This Isotherm model suggested that the adsorption of F^- on ZIF-67-NO3 occurs in multilayers and the MOF surface is heterogeneous(Nazir et al. 2022a). The maximum monolayer capacity of ZIF-67-NO3 for F^- was 25.9 mg/g according to the Langmuir model. the qmax is invaluable parameter in the Langmuir isotherm to compare the adsorptive properties of adsorbents for specific contaminants. A comparison of q_{max} for ZIF-67-NO3 and other MOFs reported in literature tabulated in Table 4. The table shows the capacity of herein studied adsorbent is in the range of many other MOFs reported earlier.

Table S4 and Fig. 6 show the parameters and illustrations of kinetic models fitted to the experiments. As seen, the coefficient of determination and adjusted R^2 is close to unity and the value of RSS is smaller for the pseudo-second-order (PSO) kinetic model compared to those of the other models. The

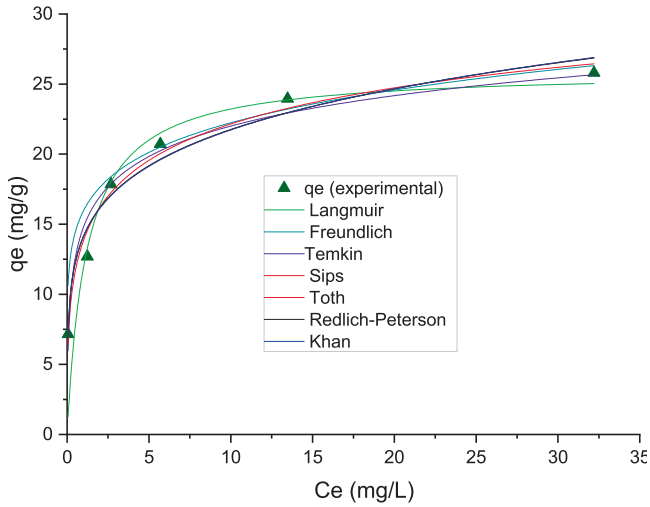

Fig. 5 Nonlinear modeling for equilibrium data of F^- adsorption.

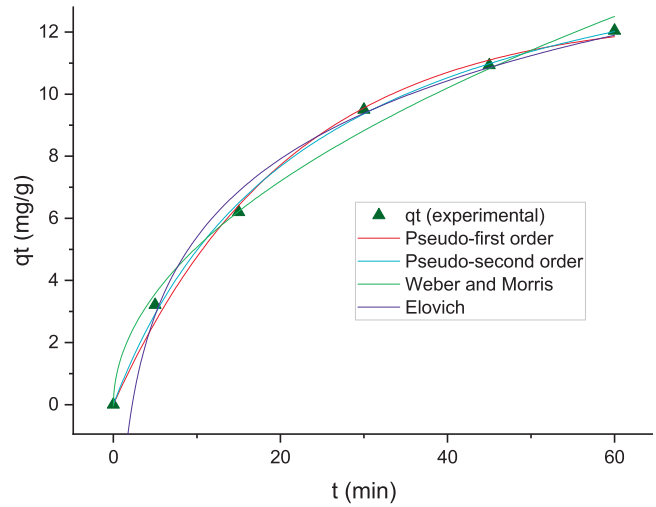

Fig. 6 Nonlinear modeling for kinetic data of F^- adsorption.

PSO kinetic model assumes the adsorption rate is controlled by the chemisorption and adsorbent-adsorbate interactions (Cao et al. 2020). Huang et al. in the study of F^- adsorption by MIL-53(Al)–NH2 also suggested the strong chemical bonding between fluoride with MOF is responsible to obey the process the PSO kinetic model (Huang et al. 2021).

3.7. Effect of temperature

Surface water and industrial discharges usually experience a wide diurnal and seasonal fluctuation in the temperature. As the temperature could affect the rate of reactions in treatment systems, it is essential to study in sorption systems. The F^- removal was determined at different solution temperatures in the range of 303 to 323 K while the operating variables were adjusted at the optimal levels i.e. mixing time = 41.1 min, ZIF-67-NO3 dose = 0.9 g/L, pH = 4.86, and F^- = 6.5 mg/L. Table 5 shows the F^- removal decreased ~ 11% by temperature which indicate the process is exothermic. Parajuli et al studied the arsenic removal onto ZIF-8 nanoparticles and found a negligible impact of temperature due to the complete dispersion of ZIF (Parajuli et al. 2018).

3.8. Regeneration studies

The regeneration of adsorbent materials after saturation with the contaminant is important to avoid excessive cost of material wastage. The reusability of adsorbent is also important in term of environmental viewpoint. Herein, the structural stability and F^- uptake ability of ZIF-67-NO3 in two consecutive cycles were studied. The adsorption of F^- accomplished at optimal condition and the exhausted material washed with DI, and regenerated by suspension in ethanol for 24 h where the solution replenished by fresh ethanol every 4 h. The removal efficiencies for pristine material and regenerated ZIF-67-NO3 given in Table 6. As seen, the removal efficiency decreased only about 10.6% after three consecutive use-reuse cycles. The exhausted ZIF-67-NO3 also analyzed by FESEM to investigate the structural stability and results presented in Fig. 7.

Table 5 F^- removal as a function of solution temperature.

Temperature (K)	303	313	323
F^- removal (%)	86.5% ± 1.9	78.6 ± 2.1	75.4 ± 2.4

Table 6 F^- removal by pristine and regenerated ZIF-67-NO3.

ZIF-67-NO3	Pristine	1st cycle	2nd cycle	3nd cycle
F^- removal (%)	86.5% ± 2.7	81.3 ± 2.6	77.6 ± 1.2	75.1 ± 1.9

Table 4 Comparison of the Langmuir qmax for F^- ZIF-67 (NO3) and studied MOFs.

Adsorbent	Q_{max} (mmol/g)	Reference	Adsorbent	Q_{max} (mmol/g)	Reference
ZIF-8	1.31	(Kamarehie et al. 2018)	MOF-801	1.02	(Tan et al. 2020)
UIO-66	1.64	(Massoudinejad et al. 2018)	UIO-66-NH2	3.09	(Lin et al. 2016)
MIL-96(Al)	2.22	(Wang et al. 2019)	Sn(II)-TMA MOF	1.62	(Ghosh &Das 2020)
MIL-53 (Fe)	3.82	(Hossien Saghi et al. 2021)	Fe-MOF	2.2	(Wang et al. 2023)
La-MOFs	5.5–9	(Yin et al. 2022)	**ZIF-67 (NO3)**	1.36	This study

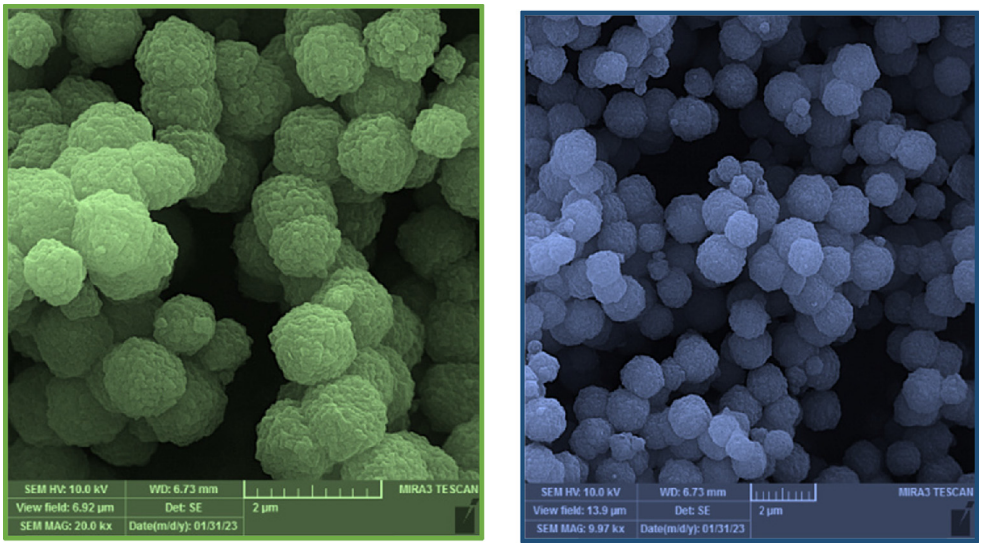

Fig. 7 The FESEM of pristine (left) and exhausted ZIF-67-NO3 (right).

4. Conclusions

Nickel, zinc, and cobalt based MOFs were studied as materials for effective removal of fluoride ions by adsorption. Adsorption efficiency of studied MOFs varied in the range of 52.3%-70.1% and ZIF-67-NO3 showed the highest adsorption efficiency. The Box-Behnken design (BBD) approach was adopted to investigate the effect of significant operating factors and their interactions on the process. The developed quadratic model predicted the removal efficiency and optimized the adsorption process for the highest efficiency. The highest F^- removal (85.9%) was achieved by adjusting mixing time, ZIF-67-NO3 dose, solution pH, and F^- concentration to 41.1 min, 0.9 g/L, 4.86, and 6.5 mg/L, respectively. Non-linear isotherm and kinetic models showed that the F^- adsorption occurs in multilayer on heterogeneously distributed sorption sites and the rate-controlling step was chemisorption. ZIF-67-NO3 has a q_{max} = 25.9 mg/g for F^- as estimated by the Langmuir model. The study also revealed the adsorption was favorable at lower temperature that indicated the exothermic nature of F^- adsorption. The F^- uptake loss of about 10.6% was observed after three consecutive use-reuse cycles, which shows great potential usefulness of the obtained materials for removal of fluride ions from waters and wastewaters.

CRediT authorship contribution statement

Amir Afarinandeh: Conceptualization, Methodology, Investigation, Formal analysis, Writing – original draft. **Kambiz Heidari:** Investigation, Methodology, Writing – review & editing. **Mariusz Barczak:** Investigation, Methodology, Writing – review & editing. **Magda H. Abdellattif:** Investigation, Methodology, Writing – review & editing. **Zahra Izadi Yazdanaabadi:** Investigation, Methodology, Writing – review & editing. **Ali Akbar Mohammadi:** Investigation, Methodology, Writing – review & editing. **Gholam Ali Haghighat:** Methodology, Writing – review & editing, Supervision. **Mahmoud Shams:** Methodology, Writing – review & editing, Supervision.

Declaration of Competing Interest

The authors declare that they have no known competing financial interests or personal relationships that could have appeared to influence the work reported in this paper.

Acknowledgments

We would like to highly appreciate the support provided by Jiroft University of Medical Sciences under grant number P_98_346.

Appendix A. Supplementary material

Supplementary data to this article can be found online at https://doi.org/10.1016/j.arabjc.2023.104837.

References

Abdelhameed, R.M., Emam, H.E., 2019. Design of ZIF(Co & Zn)@wool composite for efficient removal of pharmaceutical intermediate from wastewater. J. Colloid Interface Sci. 552, 494–505.

Acharya R, Naik B, Parida K (2018): Adsorption of Cr (VI) and textile dyes on to mesoporous silica, titanate nanotubes, and layered double hydroxides. Nanomaterials in the Wet Processing of Textiles, 219-260.

Ahamad, T., Naushad, M., Eldesoky, G.E., Al-Saeedi, S.I., Nafady, A., Al-Kadhi, N.S., AaH, A.-M., Khan, A.A., Khan, A., 2019. Effective and fast adsorptive removal of toxic cationic dye (MB) from aqueous medium using amino-functionalized magnetic multiwall carbon nanotubes. J. Mol. Liq. 282, 154–161.

Andrew Lin, K.-Y., Lee, W.-D., 2016. Self-assembled magnetic graphene supported ZIF-67 as a recoverable and efficient adsorbent for benzotriazole. Chem. Eng. J. 284, 1017–1027.

Anik, Ü., Timur, S., Dursun, Z., 2019. Metal organic frameworks in electrochemical and optical sensing platforms: a review. Microchim. Acta 186, 196.

Asgari, E., Mohammadi, F., Nourmoradi, H., Sheikhmohammadi, A., Rostamifasih, Z., Hashemzadeh, B., Arfaeinia, H., 2022. Heterogeneous catalytic degradation of nonylphenol using persulphate activated by natural pyrite: response surface methodology modelling and optimisation. Int. J. Environ. Anal. Chem. 102, 6041–6060.

Ba Mohammed, B., Hsini, A., Abdellaoui, Y., Abou Oualid, H., Laabd, M., El Ouardi, M., Ait Addi, A., Yamni, K., Tijani, N., 2020. Fe-ZSM-5 zeolite for efficient removal of basic Fuchsin dye from aqueous solutions: Synthesis, characterization and adsorption process optimization using BBD-RSM modeling. J. Environ. Chem. Eng. 8, 104419.

Bo, S., Ren, W., Lei, C., Xie, Y., Cai, Y., Wang, S., Gao, J., Ni, Q., Yao, J., 2018. Flexible and porous cellulose aerogels/zeolitic imidazolate framework (ZIF-8) hybrids for adsorption removal of Cr(IV) from water. J. Solid State Chem. 262, 135–141.

Cao, H., Wu, X., Syed-Hassan, S.S.A., Zhang, S., Mood, S.H., Milan, Y.J., Garcia-Perez, M., 2020. Characteristics and mechanisms of phosphorous adsorption by rape straw-derived biochar functionalized with calcium from eggshell. Bioresour. Technol. 318, 124063.

Chueh, C.-C., Chen, C.-I., Su, Y.-A., Konnerth, H., Gu, Y.-J., Kung, C.-W., Wu, K.-C.-W., 2019. Harnessing MOF materials in photovoltaic devices: recent advances, challenges, and perspectives. J. Mater. Chem. A 7, 17079–17095.

Council NR (2007): Fluoride in drinking water: a scientific review of EPA's standards.

Dehghan, A., Mohammadi, A.A., Yousefi, M., Najafpoor, A.A., Shams, M., Rezania, S., 2019. Enhanced kinetic removal of ciprofloxacin onto metal-organic frameworks by sonication, process optimization and metal leaching study. Nanomaterials 9, 1422.

Edition, F., 2011. Guidelines for drinking-water quality. WHO Chron. 38, 104–108.

Esrafili, A., Ghambarian, M., Yousefi, M., 2022. Electrospun zeolitic imidazolate framework-8/poly (lactic acid) nanofibers for pipette-tip micro-solid phase extraction of carbamate insecticides from environmental samples. Arab. J. Chem. 15, 104124.

Feng, M., Zhang, P., Zhou, H.-C., Sharma, V.K., 2018. Water-stable metal-organic frameworks for aqueous removal of heavy metals and radionuclides: a review. Chemosphere 209, 783–800.

Gholamiyan, S., Hamzehloo, M., Farrokhnia, A., 2020. RSM optimized adsorptive removal of erythromycin using magnetic activated carbon: adsorption isotherm, kinetic modeling and thermodynamic studies. Sustain. Chem. Pharm. 17, 100309.

Ghosh, A., Das, G., 2020. Green synthesis of a novel water-stable Sn (ii)-TMA metal–organic framework (MOF): an efficient adsorbent for fluoride in aqueous medium in a wide pH range. New J. Chem. 44, 1354–1361.

Guo, X., Xing, T., Lou, Y., Chen, J., 2015. Controlling ZIF-67 crystals formation through various cobalt sources in aqueous solution. J. Solid State Chem. 235.

Haghighat, G.A., Sadeghi, S., Saghi, M.H., Ghadiri, S.K., Anastopoulos, I., Giannakoudakis, D.A., Colmenares, J.C., Shams, M., 2020. Zeolitic imidazolate frameworks (ZIFs) of various morphologies against eriochrome black-T (EBT): optimizing the key physicochemical features by process modeling. Colloids Surf. A Physicochem. Eng. Asp. 606, 125391.

Hossien Saghi, M., Chabot, B., Rezania, S., Sillanpää, M., Akbar Mohammadi, A., Shams, M., Alahabadi, A., 2021. Water-stable zirconium and iron-based metal-organic frameworks (MOFs) as fluoride scavengers in aqueous medium. Sep. Purif. Technol. 270, 118645.

Huang, J., Fang, G., Liu, K., Zhou, J., Tang, X., Cai, K., Liang, S., 2017. Controllable synthesis of highly uniform cuboid-shape MOFs and their derivatives for lithium-ion battery and photocatalysis applications. Chem. Eng. J. 322, 281–292.

Huang, L., Yang, Z., Li, X., Hou, L., Alhassan, S.I., Wang, H., 2021. Synthesis of hierarchical hollow MIL-53(Al)-NH2 as an adsorbent for removing fluoride: experimental and theoretical perspective. Environ. Sci. Pollut. Res. 28, 6886–6897.

Kamarehie, B., Noraee, Z., Jafari, A., Ghaderpoori, M., Karami, M. A., Ghaderpoury, A., 2018. Data on the fluoride adsorption from aqueous solutions by metal-organic frameworks (ZIF-8 and Uio-66). Data Brief 20, 799–804.

Karunanithi, M., Agarwal, R., Qanungo, K., 2019. A review of fluoride removal from groundwater. Period. Polytech., Chem. Eng. 63, 425–437.

Khan, A., Ali, M., Ilyas, A., Naik, P., Vankelecom, I.F.J., Gilani, M. A., Bilad, M.R., Sajjad, Z., Khan, A.L., 2018. ZIF-67 filled PDMS mixed matrix membranes for recovery of ethanol via pervaporation. Sep. Purif. Technol. 206, 50–58.

Khan, N.A., Shaheen, S., Najam, T., Shah, S.S.A., Javed, M.S., Nazir, M.A., Hussain, E., Shaheen, A., Hussain, S., Ashfaq, M., 2021. Efficient removal of norfloxacin by MOF@ GO composite: isothermal, kinetic, statistical, and mechanistic study. Toxin Rev. 40, 915–927.

Khoshnamvand, N., Jafari, A., Kamarehie, B., Faraji, M., 2019. Optimization of adsorption and sonocatalytic degradation of fluoride by zeolitic imidazole framework-8 (ZIF-8) using RSM-CCD. Desalin. Water Treat. 171, 270–280.

Konnerth, H., Matsagar, B.M., Chen, S.S., Prechtl, M.H., Shieh, F.-K., Wu, K.-C.-W., 2020. Metal-organic framework (MOF)-derived catalysts for fine chemical production. Coord. Chem. Rev. 416, 213319.

Kumar, O.P., Ahmad, M., Nazir, M.A., Anum, A., Jamshaid, M., Shah, S.S.A., Rehman, A., 2022. Strategic combination of metal–organic frameworks and C3N4 for expeditious photocatalytic degradation of dye pollutants. Environ. Sci. Pollut. Res. 29, 35300–35313.

Li, H., Li, X., Chen, Y., Long, J., Zhang, G., Xiao, T., Zhang, P., Li, C., Zhuang, L., Huang, W., 2018. Removal and recovery of thallium from aqueous solutions via a magnetite-mediated reversible adsorption-desorption process. J. Clean. Prod. 199, 705–715.

Li, J., Wu, Z., Duan, Q., Li, X., Li, Y., Alsulami, H., Alhodaly, M.S., Hayat, T., Sun, Y., 2020. Simultaneous removal of U(VI) and Re (VII) by highly efficient functionalized ZIF-8 nanosheets adsorbent. J. Hazard. Mater. 393, 122398.

Liang, C., Zhang, X., Feng, P., Chai, H., Huang, Y., 2018. ZIF-67 derived hollow cobalt sulfide as superior adsorbent for effective adsorption removal of ciprofloxacin antibiotics. Chem. Eng. J. 344, 95–104.

Lin, K.-Y.-A., Chang, H.-A., 2015. Ultra-high adsorption capacity of zeolitic imidazole framework-67 (ZIF-67) for removal of malachite green from water. Chemosphere 139, 624–631.

Lin, K.-Y.-A., Liu, Y.-T., Chen, S.-Y., 2016. Adsorption of fluoride to UiO-66-NH2 in water: stability, kinetic, isotherm and thermodynamic studies. J. Colloid Interface Sci. 461, 79–87.

Liu, B., Jian, M., Liu, R., Yao, J., Zhang, X., 2015a. Highly efficient removal of arsenic (III) from aqueous solution by zeolitic imidazolate frameworks with different morphology. Colloids Surf. A Physicochem. Eng. Asp. 481, 358–366.

Liu, B., Jian, M., Liu, R., Yao, J., Zhang, X., 2015b. Highly efficient removal of arsenic(III) from aqueous solution by zeolitic imidazolate frameworks with different morphology. Colloids Surf. A Physicochem. Eng. Asp. 481, 358–366.

Liu, Y.-C., Yeh, L.-H., Zheng, M.-J., Wu, K.-C.-W., 2021. Highly selective and high-performance osmotic power generators in subnanochannel membranes enabled by metal-organic frameworks. Sci. Adv. 7, eabe9924.

Massoudinejad, M., Ghaderpoori, M., Shahsavani, A., Amini, M.M., 2016. Adsorption of fluoride over a metal organic framework Uio-66 functionalized with amine groups and optimization with response surface methodology. J. Mol. Liq. 221, 279–286.

Massoudinejad, M., Shahsavani, A., Kamarehie, B., Jafari, A., Ghaderpoori, M., Amini, M.M., Ghaderpoury, A., 2018. Highly efficient adsorption of fluoride from aqueous solutions by metal organic frameworks: modeling, isotherms, and kinetics. Fluoride 51, 355–365.

Mazloomi, S., Yousefi, M., Nourmoradi, H., Shams, M., 2019. Evaluation of phosphate removal from aqueous solution using metal organic framework; isotherm, kinetic and thermodynamic study. J. Environ. Health Sci. Eng. 17, 209–218.

Moghaddam, V.K., Yousefi, M., Khosravi, A., Yaseri, M., Mahvi, A. H., Hadei, M., Mohammadi, A.A., Robati, Z., Mokammel, A., 2018. High concentration of fluoride can be increased risk of abortion. Biol. Trace Elem. Res. 185, 262–265.

Mohammadi, A., Nemati, S., Mosaferi, M., Abdollahnejhad, A., Almasian, M., Sheikhmohammadi, A., 2017a. Predicting the capability of carboxymethyl cellulose-stabilized iron nanoparticles

for the remediation of arsenite from water using the response surface methodology (RSM) model: modeling and optimization. J. Contam. Hydrol. 203, 85–92.

Mohammadi, A.A., Yousefi, M., Yaseri, M., Jalilzadeh, M., Mahvi, A. H., 2017b. Skeletal fluorosis in relation to drinking water in rural areas of West Azerbaijan, Iran. Scient. Rep. 7, 1–7.

Mohapatra, M., Anand, S., Mishra, B.K., Giles, D.E., Singh, P., 2009. Review of fluoride removal from drinking water. J. Environ. Manage. 91, 67–77.

Nazir MA, Khan NA, Cheng C, Shah SSA, Najam T, Arshad M, Sharif A, Akhtar S, ur Rehman A (2020): Surface induced growth of ZIF-67 at Co-layered double hydroxide: Removal of methylene blue and methyl orange from water. Applied Clay Science 190, 105564

Nazir MA, Najam T, Jabeen S, Wattoo MA, Bashir MS, Shah SSA, ur Rehman A (2022b): Facile synthesis of Tri-metallic layered double hydroxides (NiZnAl-LDHs): Adsorption of Rhodamine-B and methyl orange from water. Inorganic Chemistry Communications 145, 110008

Nazir MA, Najam T, Shahzad K, Wattoo MA, Hussain T, Tufail MK, Shah SSA, ur Rehman A (2022c): Heterointerface engineering of water stable ZIF-8@ ZIF-67: Adsorption of rhodamine B from water. Surfaces and Interfaces 34, 102324

Nazir, M.A., Najam, T., Zarin, K., Shahzad, K., Javed, M.S., Jamshaid, M., Bashir, M.A., Shah, S.S.A., Rehman, A.U., 2021. Enhanced adsorption removal of methyl orange from water by porous bimetallic Ni/Co MOF composite: a systematic study of adsorption kinetics. Int. J. Environ. Anal. Chem., 1–16

Nazir, M.A., Najam, T., Bashir, M.S., Javed, M.S., Bashir, M.A., Imran, M., Azhar, U., Shah, S.S.A., Rehman, A.u., 2022a. Kinetics, isothermal and mechanistic insight into the adsorption of eosin yellow and malachite green from water via tri-metallic layered double hydroxide nanosheets. Korean J. Chem. Eng. 39, 216–226.

Nezhad, N.T., Shams, M., Dehghan, A., Aziznezhad, M., Goharshadi, E.K., Mohammadhosseini, F., Wilson, L.D., 2020. Vanadium dioxide nanoparticles as a promising sorbent for controlled removal of waterborne fluoroquinolone ciprofloxacin. Mater. Chem. Phys., 123993

Oveisi, M., Asli, M.A., Mahmoodi, N.M., 2018. MIL-Ti metal-organic frameworks (MOFs) nanomaterials as superior adsorbents: synthesis and ultrasound-aided dye adsorption from multicomponent wastewater systems. J. Hazard. Mater. 347, 123–140.

Parajuli, D., Sue, K., Takahashi, A., Tanaka, H., Kawamoto, T., 2018. Adsorption of ng L− 1-level arsenic by ZIF-8 nanoparticles: application to the monitoring of environmental water. RSC Adv. 8, 36360–36368.

Pillai, P., Dharaskar, S., Sasikumar, S., Khalid, M., 2019. Zeolitic imidazolate framework-8 nanoparticle: a promising adsorbent for effective fluoride removal from aqueous solution. Appl. Water Sci. 9, 150.

Rasoulzadeh, H., Dehghani, M.H., Mohammadi, A.S., Karri, R.R., Nabizadeh, R., Nazmara, S., Kim, K.-H., Sahu, J.N., 2020. Parametric modelling of Pb(II) adsorption onto chitosan-coated Fe3O4 particles through RSM and DE hybrid evolutionary optimization framework. J. Mol. Liq. 297, 111893.

Rasoulzadeh, H., Sheikhmohammadi, A., Abtahi, M., Roshan, B., Jokar, R., 2021a. Eco-friendly rapid removal of palladium from aqueous solutions using alginate-diatomite magnano composite. J. Environ. Chem. Eng. 9, 105954.

Rasoulzadeh, H., Sheikhmohammadi, A., Asgari, E., Hashemzadeh, B., 2021b. The adsorption behaviour of triclosan onto magnetic bio polymer beads impregnated with diatomite. Int. J. Environ. Anal. Chem., 1–13

Safaei, M., Foroughi, M.M., Ebrahimpoor, N., Jahani, S., Omidi, A., Khatami, M., 2019. A review on metal-organic frameworks: synthesis and applications. TrAC Trends Anal. Chem. 118, 401–425.

Saghi, M.H., Qasemi, M., Alidadi, H., Alahabadi, A., Rastegar, A., Kowsari, M.H., Shams, M., Aziznezhad, M., Goharshadi, E.K., Barczak, M., Anastopoulos, I., Giannakoudakis, D.A., 2020. Vanadium oxide nanoparticles for methylene blue water remediation: exploring the effect of physicochemical parameters by process modeling. J. Mol. Liq. 318, 114046.

Shah, S.S.A., El Jery, A., Najam, T., Nazir, M.A., Wei, L., Hussain, E., Hussain, S., Rebah, F.B., Javed, M.S., 2022. Surface engineering of MOF-derived FeCo/NC core-shell nanostructures to enhance alkaline water-splitting. Int. J. Hydrogen Energy 47, 5036–5043.

Soltani, R., Marjani, A., Shirazian, S., 2019. Facile one-pot synthesis of thiol-functionalized mesoporous silica submicrospheres for Tl (I) adsorption: isotherm, kinetic and thermodynamic studies. J. Hazard. Mater. 371, 146–155.

Song, Y., Seo, J.Y., Kim, H., Beak, K.-Y., 2019. Structural control of cellulose nanofibrous composite membrane with metal organic framework (ZIF-8) for highly selective removal of cationic dye. Carbohydr. Polym. 222, 115018.

Tan, T.L., Krusnamurthy, P.A.P., Nakajima, H., Rashid, S.A., 2020. Adsorptive, kinetics and regeneration studies of fluoride removal from water using zirconium-based metal organic frameworks. RSC Adv. 10, 18740–18752.

Till, C., Green, R., Flora, D., Hornung, R., Martinez-Mier, E.A., Blazer, M., Farmus, L., Ayotte, P., Muckle, G., Lanphear, B., 2020. Fluoride exposure from infant formula and child IQ in a Canadian birth cohort. Environ. Int. 134, 105315.

Van Nguyen, C., Yeh, J.-Y., Van Tran, T., Wu, K.-C.-W., 2022. Highly efficient one-pot conversion of saccharides to 2, 5-dimethylfuran using P-UiO-66 and Ni–Co@ NC noble metal-free catalysts. Green Chem. 24, 5070–5076.

Wang W, Huang Y, Han G (2023): Application Study of Fe-MOF Material for Fluoride Removal from Hydrometallurgy Waste Liquid, TMS 2023 152nd Annual Meeting & Exhibition Supplemental Proceedings. Springer, pp. 707-714.

Wang, X., Zhu, H., Sun, T., Liu, Y., Han, T., Lu, J., Dai, H., Zhai, L., 2019. Synthesis and study of an efficient metal-organic framework adsorbent (MIL-96(Al)) for fluoride removal from water. J. Nanomater. 2019, 3128179.

Yang M, Bai Q (2019): Flower-like hierarchical Ni-Zn MOF microspheres: Efficient adsorbents for dye removal. Colloids and Surfaces A: Physicochemical and Engineering Aspects 582, 123795.

Yang K, Liang X (2011): Fluoride in drinking water: effect on liver and kidney function.

Yang, R.-X., Bieh, Y.-T., Chen, C.H., Hsu, C.-Y., Kato, Y., Yamamoto, H., Tsung, C.-K., Wu, K.-C.-W., 2021. Heterogeneous metal azolate framework-6 (MAF-6) catalysts with high zinc density for enhanced polyethylene terephthalate (PET) conversion. ACS Sustain. Chem. Eng. 9, 6541–6550.

Yang, Y., Li, X., Gu, Y., Lin, H., Jie, B., Zhang, Q., Zhang, X., 2022. Adsorption property of fluoride in water by metal organic framework: optimization of the process by response surface methodology technique. Surf. Interfaces 28, 101649.

Yin, C., Huang, Q., Zhu, G., Liu, L., Li, S., Yang, X., Wang, S., 2022. High-performance lanthanum-based metal–organic framework with ligand tuning of the microstructures for removal of fluoride from water. J. Colloid Interface Sci. 607, 1762–1775.

Zhu, X.-H., Yang, C.-X., Yan, X.-P., 2018. Metal-organic framework-801 for efficient removal of fluoride from water. Micropor. Mesopor. Mater. 259, 163–170.